Nanoscale

PAPER

View Article Online
View Journal

Cite this: DOI: 10.1039/d6nr00693k

Unravelling the structure of broadband white-emitting silver nanoclusters stabilized in sulfur-doped zeolites

José Adán Moreno-Torres,[a] Catarina Viola,[b,c] Francesco D'Acapito,[d] Paul Thompson,[e] Andreia Ruivo,[c] César A. T. Laia,[b,c] Peter Lievens,[f] Eduardo Coutiño-Gonzalez*[g] and Didier Grandjean*[f]

The unclear origin of the photoluminescence (PL) in single-phase white-light materials based on silver nanoclusters (Ag–NCs) confined within zeolite hosts has hindered the rational design of composites with tunable emission properties. In this study, we combined X-ray Excited Optical Luminescence (XEOL)–X-ray Absorption Fine Structure (XAFS) at the silver K-edge and X-ray Absorption Near Edge Structure (XANES) at the sulfur K-edge to unravel the structure of the species responsible for the white emission in Ag/S-SOD zeolites. Our findings reveal that the white luminescence observed in these materials arises from the formation and stabilization within the sodalite cages of a mixture of Ag_3O, Ag_4O_2, and Ag_6O_4 NCs coordinated by oxygen ligands, each having specific emission features. The precise tone of the white-light emission can be further tuned by adjusting their relative fractions. The remarkable emission stability of these materials originates from the closed structure of the SOD zeolites and the formation of a network of Ag–NCs and co-cations stabilized by oxygen ligands, whose coordination environment is modulated by transient silver–sulfur interactions occurring during synthesis. Ultimately, Ag/S-SOD zeolites are not only efficient single-phase and emission-tunable phosphors but also robust platforms for studying the structure–property relationships of confined metal NCs.

Received 16th February 2026,
Accepted 29th April 2026

DOI: 10.1039/d6nr00693k

rsc.li/nanoscale

Introduction

The current quest for novel single-phase and emission-tunable phosphors is driven by their promising potential applications as near-ultraviolet (NUV)-converted white light-emitting diodes (WLEDs). However, current commercial WLEDs based on YAG phosphors lack red components, making the development of novel warm-white-light phosphors activated by NUV light highly desirable. Encapsulating guest-emitting species within an inorganic host/scaffold has proven to be an effective strategy for tuning their optical properties and improving their stability. A wide range of guest species ranging from dyes,[1] organic molecules,[2] lanthanides,[3] quantum dots,[4] carbon dots,[5] perovskites,[6] to metal nanoclusters (NCs)[7] have been investigated, whereas micro(meso)porous materials such as metal–organic frameworks[8] and zeolites[9,10] have successfully demonstrated their potential as versatile confinement scaffolds. Among these, luminescent few-atom Ag–NCs confined inside a porous zeolite have attracted considerable interest due to their fascinating molecule-like properties,[9,11] which include high quantum yields and emission tunability across the visible spectrum. Their optical features can be fine-tuned and optimized for specific applications by taking advantage of their high susceptibility to external stimuli and changes in their local environment.[12,13]

Several strategies have been explored to develop single-phase white phosphors based on Ag–NC-zeolite composites. One approach involves the formation and stabilization of Ag–NCs within Faujasite (FAU)-Y zeolites by calcining the Ag-exchanged zeolite at various temperatures. The white emission obtained at 950 °C was attributed to interactions occurring between the two species $(Ag_2)^+$–$(Ag^+)_2$ formed during the zeolite collapse at this high temperature.[14] Alternatively, in

[a]Centro de Física Aplicada y Tecnología Avanzada, Universidad Nacional Autónoma de México, Boulevard Juriquilla 3001, Juriquilla, Santiago de Querétaro, 76230 Querétaro, Mexico
[b]LAQV@REQUIMTE, Chemistry Department, NOVA School of Science and Technology (NOVA FCT), 2829-516 Caparica, Portugal
[c]Research Unit VICARTE, Vidro e Cerâmica para as Artes, NOVA School of Science and Technology (NOVA FCT), 2829-516 Caparica, Portugal
[d]Consiglio Nazionale delle Ricerche – Istituto Officina dei Materiali – Operative Group in Grenoble (CNR-IOM-OGG), The European Synchrotron (ESRF) LISA Collaborating Research Group, 71, avenue des Martyrs, 38043 Grenoble, France
[e]XMaS UK CRG Beamline, ESRF – The European Synchrotron, 71, avenue des Martyrs, 38043 Grenoble, France
[f]Quantum Solid State Physics, KU Leuven, Celestijnenlaan 200D, 3001 Leuven, Belgium. E-mail: didier.grandjean@kuleuven.be
[g]Interuniversity Microelectronics Center (imec), Kapeldreef 75, 3001 Leuven, Belgium. E-mail: eduardo.coutinogonzalez@imec.be

flexible small-pore zeolites such as Ag-exchanged NaP1, the emission was tuned from violet and blue-white to bright white by varying the Ag loading. This effect was attributed to the ability of the zeolite structure to stabilize concomitantly two types of Ag–NCs, tentatively assigned to Ag_3 and Ag_4^{2+}, respectively, displaying emission bands in the blue (458 nm) and yellow-green (570 nm) regions, whose interplay results in the observed white-light emission.[15]

The sodalite (SOD) zeolite has also been used for stabilizing Ag–NCs. In Ag-exchanged SOD, white emission was achieved by simultaneously optimizing the Ag loading, the type of extra-framework co-cation (*e.g.*, Li^+, Na^+, K^+, Cs^+, Mg^{2+}, and Ca^{2+}), and the heat-treatment temperature. As luminescence in these materials is significantly influenced by the type of co-cation, Ag–NC-based emissions ranging from blue to orange were typically observed, while white emission was exclusively observed in K-SOD samples treated below 500 °C. These changes were attributed to the shrinkage of the zeolite crystal unit cell induced by the different co-cations.[16] This structural contraction subtly alters the excited-state geometry and electronic environment of the confined Ag–NCs, leading to changes in their emission-color without modification of their nuclearity.[13]

Beyond compositional tuning, co-doping with Zn^{2+} and Eu^{3+} ions has also been explored to modulate the emission in Ag–NC-SOD systems. Warm-white PL was achieved through an energy-transfer mechanism from few-atom Ag–NCs $(Ag_2)^{n+}$ to the Eu^{3+} centers, combined with the spectral overlap of the respective green and red emissions of Ag–NCs and Eu^{3+}.[17] These findings highlight the potential application of SOD zeolites as white-emitting materials *via* co-doping strategies. Nevertheless, the cost, scarcity, and negative environmental impact of rare-earth elements emphasize the need for more accessible and sustainable alternatives.[18]

In this context, chalcogenides, particularly sulfur (S), have gained attention as co-dopants due to their natural abundance, low toxicity, and reduced environmental impact, making them a viable alternative to rare-earth-based systems.[19] Baekelant and co-workers[20] synthesized Ag/S-zeolites with broadband white emission by adapting a procedure from the study by Ruivo *et al.*[21] involving a solid-state reaction of Linde Type A (LTA) zeolite precursors with Na_2SO_4 and NaCl under a reducing atmosphere at high temperatures. Emissions in the orange region (low S content) and red-NIR region (high S content), tentatively attributed to S_2^- and S_3^{2-} centers, were observed, respectively.[19,21] They also demonstrated that PL species only form under mild reducing conditions, while a more aggressive reduction produces S_2^{2-} centers associated with a photochromic (PC) behavior. A subsequent cation exchange with Ag^+ produced highly stable zeolite phosphors with broadband white emission. The emission color could be tuned from cold to warm white by varying the synthesis and heat-treatment conditions, which control the relative fractions of luminescent Ag–NCs and S-species within the SOD framework. This tunability suggests the coexistence of multiple emitting centers within the same structure. However, due to the lack of detailed structural information, the origin of the white emission was not fully understood.

To further advance the design of white light-emitting single-phase SOD zeolites, a detailed understanding of the atomic structure of the luminescent Ag–NCs produced through Ag^+ cation exchange in PL-SOD zeolite-S composites was obtained by X-ray Absorption Fine Structure (XAFS) spectroscopy at the Ag K-edge, directly detected by the modulation of the X-ray Excited Optical Luminescence (XEOL) of the material. This innovative approach provides deeper structural insight, offering a better understanding of the emitting species and the Ag–NC ligands, aspects not fully explored in previous studies.[20] Specifically, XEOL–XAFS enables measuring exclusively the local structure around the Ag atoms generating the luminescence, facilitating the identification of the Ag–NC emitting species confined in the zeolite. Unlike the single-crystal diffraction technique, XAFS can be performed on powdered samples and does not rely on long-range order that requires atoms to occupy strict crystallographic positions, a requirement generally not fulfilled by Ag atoms forming clusters within the zeolite cages.[11] This was complemented by X-ray Absorption Near Edge Structure (XANES) spectra collected at the S K-edge to identify the sulfur species present within the SOD framework, providing additional insights into the chemical changes leading to the formation of the white light-emitting material. Our findings establish the basis for a precise structural identification of single-phase white light-emitting Ag–NCs confined within complex inorganic matrices.

Methodology

PC-SOD and PL-SOD zeolite-S composites were synthesized following a procedure described elsewhere,[21] using nominal molar ratios of S/Cl between 0.21 and 0.33 to ensure a well-defined S content, as S loading critically influences the optical properties of the resulting materials. Subsequently, ion exchanges with Ag^+ ions were conducted using $AgNO_3$ solutions, following two synthetic routes resulting in three samples labeled W_W@Ag/S, W_B@Ag/S, and W_R@Ag/S, reflecting their respective white–white, white–blue, and white–red emission colors. The selection of these samples is based on a broader optimization study,[20] in which variations in synthesis and heat-treatment conditions were found to control the formation of distinct emissive species. The three selected samples therefore represent characteristic emission regimes associated with different NC distributions. For the W_W@Ag/S sample, 200 mg of as-synthesized PL-SOD were ground using a mortar and pestle and then exchanged with 20 mg of $AgNO_3$ dissolved in 200 mL of Milli-Q (MQ) water corresponding to a nearly fully exchange of the original Na^+ co-cations. The mixture was stirred overnight in an end-over-end shaking oven in the dark, filtered, and dried at 50 °C for 1 h. While a similar ion exchange procedure was followed to synthesize W_B@Ag/S and W_R@Ag/S samples, the former was heat-treated at 250 °C overnight instead of being simply dried at 50 °C, whereas the latter was prepared omitting the grinding step. Additionally, a reference sample consisting of S-free SOD zeolites exchanged with

Ag^+ ions (SOD-Ag) was synthesized following a procedure described elsewhere.[20] The steady-state luminescence properties, including the two-dimensional (2D) excitation–emission plots, were recorded using an Edinburgh FLS980 fluorimeter.

XAFS spectra of heat-treated samples were collected at the Ag K-edge (E = 25 514 eV) simultaneously in transmission and XEOL detection modes at the GILDA beamline (BM08)[22] of The European Synchrotron (ESRF, Grenoble, France), operating in a 7/8 +1 filling mode with a current of 200 mA. The monochromator had a first flat crystal and a second sagittally bent crystal and was run in the dynamical-focusing mode using Si (111) crystals cooled with water. Harmonic rejection was performed using a pair of Pt-coated mirrors ($E_{cutoff} \approx 32$ keV). The ionization chambers for transmission measurements were filled with Ar gas at 1 atm. An Ag foil was placed after the second ion chamber and measured together with the sample in order to check the stability of the energy scale. XEOL emission from the sample was collected by two lenses (BK7 glass) and sent, through an optical fiber, to a photomultiplier tube (pulse duration <2 ns) with sensitivity in the range of 300–650 nm. The samples were measured under ambient conditions up to a k = 13 $Å^{-1}$ wave number with a typical acquisition time of 35 min (*i.e.*, 5–20 s per data point). Eight spectra were averaged to improve the signal-to-noise ratio of the XEOL-detected spectra. Despite the relatively weak XEOL signal, a reliable EXAFS signal could still be obtained up to k = 8 $Å^{-1}$.

Data reduction of the experimental X-ray absorption spectra was performed using the EXBROOK program.[23] Background subtraction and normalization were carried out by fitting (i) a linear polynomial to the pre-edge region to remove any instrumental background and (ii) cubic splines simulating the absorption coefficient from an isolated atom to the post-edge region. EXAFS refinements were performed using the EXCURVE package.[23] Phase shifts and backscattering factors were calculated *ab initio* using Hedin–Lundqvist potentials. Although the data were fitted in both k^2 and k^3 spaces, k^3 weighting was applied during the fitting to increase the sensitivity to heavy atoms such as Ag and to enhance the high k-range of the spectra.

XANES spectra were measured at the S K-edge (2472 eV) in fluorescence yield at BM28 (XMaS – The UK-CRG, ESRF)[24] in a uniform filling mode, before the ESRF EBS/XMaS upgrade program in 2020. The beamline was equipped with a water-cooled Si(111) monochromator and a single rhodium-coated toroidal mirror, with an incidence angle of 4.5 mrad, providing an energy cut-off of approximately 15 keV, with the lower energy limit of 2.4 keV determined by the monochromator geometry. The samples were placed in a vacuum chamber, with a base pressure of approximately 1 × 10^{-6} mbar and connected to the beamline vacuum system. This eliminated any air absorption and maximized the fluorescence signal from the sample. All spectra were acquired using a Ketek Silicon Drift Diode and processed using a Mercury XIA digital signal processor.

Results and discussion

The 2D excitation–emission plot (Fig. 1A) of the most representative Ag-loaded W_W@Ag/S sample displays a broad emission centered around 485 nm under 340 nm excitation. Two additional minor peaks are also observed: one broad emission with a maximum at 505 nm under 310 nm excitation and a reddish-orange emission peaking at 630 nm when excited at 395 nm. Compared to W_W@Ag/S, the other samples W_B@Ag/S, W_R@Ag/S, and SOD-Ag exhibit distinct emission behaviors characterized by variations in peak positions and spectral shapes. These differences suggest significant variations in the types and distributions of emissive Ag species present in each sample. The 2D excitation–emission plots highlighting the key

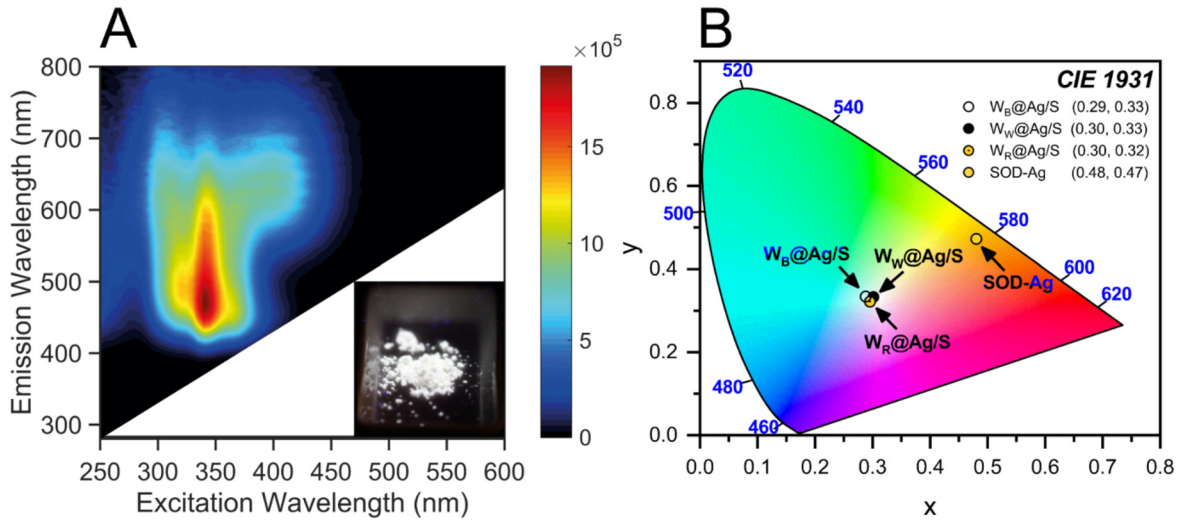

Fig. 1 (A) 2D excitation–emission plot of the W_W@Ag/S sample; inset: picture of the W_W@Ag/S sample under 366 nm UV illumination. (B) CIE chromaticity coordinates of Ag/S zeolite composites under 340 nm excitation.

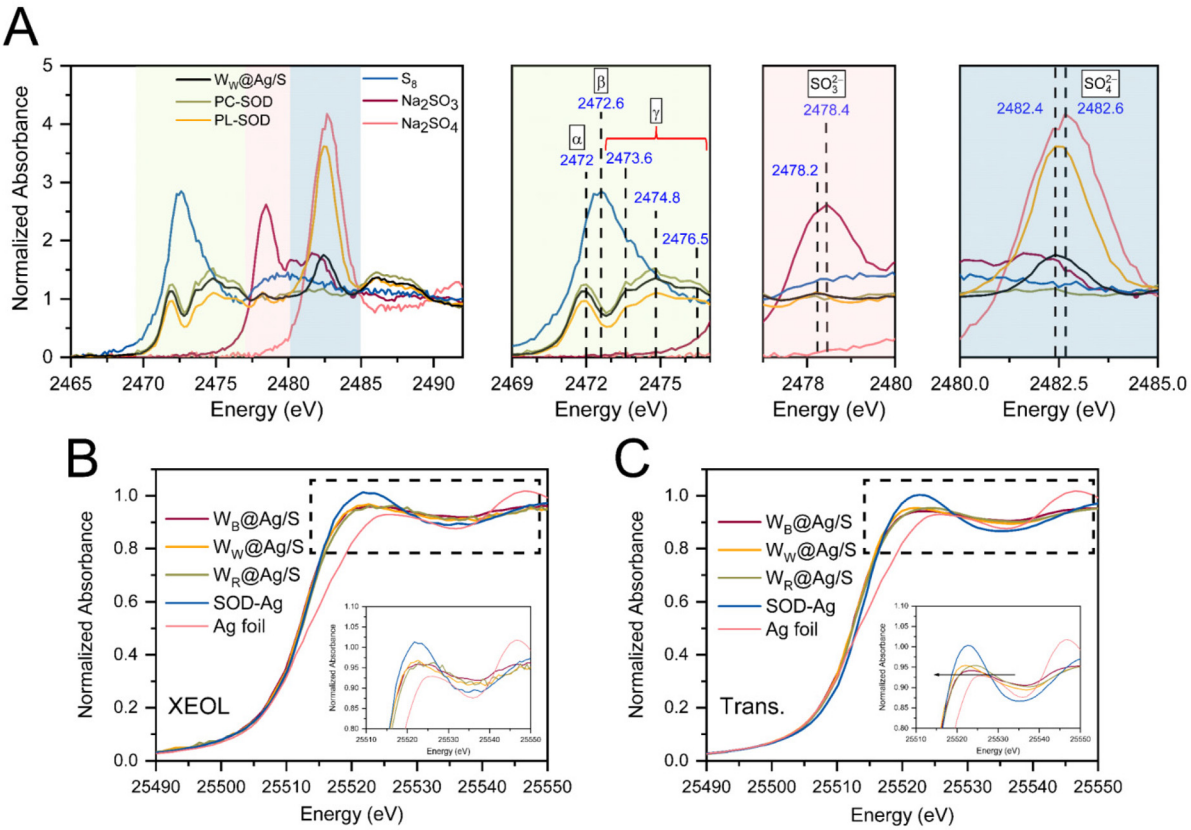

Fig. 2 (A) S K-edge XANES spectra of PL-SOD, PC-SOD, and W_W@Ag/S along with references S_8, Na_2SO_3, and Na_2SO_4. The inset highlights the 2469–2478 eV region in which the labels correspond to the following tentative assignments: anions (α), elemental S (β), and radical species (γ);[25,26] (B) XEOL and (C) transmission-detected Ag K-edge XANES spectra of W_B@Ag/S, W_W@Ag/S, W_R@Ag/S, and SOD-Ag along with reference Ag foil.

spectral changes resulting from the presence of blue- and red-orange-emitting species in the samples are depicted in the SI (Fig. S1).

The corresponding CIE chromaticity coordinates for the SOD-Ag, W_W@Ag/S, W_R@Ag/S, and W_B@Ag/S samples, excited at 340 nm, are presented in Fig. 1B. Depending on the synthesis and heat-treatment conditions, the emissions of W_W@Ag/S, W_B@Ag/S, and W_R@Ag/S all appear in the white region of the CIE diagram. In contrast, the SOD-Ag emission is found in a more yellowish-orange region, suggesting that S influences the emission color. Notably, W_W@Ag/S is positioned at (0.30, 0.33), which closely matches the ideal coordinates for pure white emission (0.33, 0.33).

S K-edge XANES

To investigate the electronic properties of the S species confined within the SOD, XANES spectra of the different samples were collected at the S K-edge. This technique, which is sensitive to the oxidation state and the atomic coordination of S species, provides detailed insights into S speciation within the zeolite framework. S K-edge XANES spectra of PC-SOD and PL-SOD precursors, before and after Ag exchange (W_W@Ag/S), along with those of S_8, Na_2SO_3, and Na_2SO_4 reference compounds, are presented in Fig. 2A.

The PC-SOD spectrum shows a notable similarity to natural[25] and synthetic[26] hackmanite samples, which are known to stabilize S species in multiple oxidation states, encompassing both reduced and oxidized forms. In the 2469–2478 eV range (inset, Fig. 2A, where peaks are labeled as α, β, and γ), a prominent white line (WL) peak is observed at 2472 eV (α), accompanied by a set of three consecutive peaks at 2473.6, 2474.8, and 2476.5 eV (γ).[25] The peak at 2472 eV (α) lying very close to the reference value for S_8 (2472.6 eV, labeled as β), corresponds to elemental S.[25] The fact that its spectral profile differs significantly from that of S_8 suggests that the S atoms in this sample may adopt a non-circular structure. The three consecutive peaks (γ) have often been attributed to reduced S species, analogous to those reported in hackmanites.[25,26] These reduced S species, which may play an essential role in the optical properties of the PL-SOD and PC-SOD precursors, are consistent with the formation of multiple radical sulfur anions. They remain stable upon Ag exchange, as shown by the similarity of the XANES profiles in this region in Ag/S-SOD and in both SOD precursors.

Although mostly similar to that of its PC-SOD counterpart, the XANES profile of PL-SOD exhibits two additional peaks (insets,

Fig. 2A): a weak one around 2478.2 eV, close to the characteristic WL position of Na_2SO_3 (2478.4 eV), typically associated with sulfite species (SO_3^{2-});[27] and a more intense one at 2482.4 eV, near the WL position of the Na_2SO_4 reference (2482.6 eV), attributed to sulfate (SO_4^{2-}),[25,28] indicating the presence of significant amounts of these species within the sodalite cage. The SO_4^{2-} species may originate from the Na_2SO_4 precursor used during the SOD synthesis, while SO_3^{2-} may be an intermediate species formed during the early stages of the SO_4^{2-} reduction. Furthermore, in PC-SOD, the prolonged reduction described in the synthesis procedure elsewhere[21] favors the conversion of SO_4^{2-} to S_2^{2-} species, which could explain the disappearance of the SO_4^{2-} peak observed in this sample.

Ag exchange of PL-SOD to form W_W@Ag/S results in an abrupt decrease in the SO_4^{2-} peak intensity at 2482.4 eV (inset, Fig. 2A), indicating a sharp reduction in the amount of sulfate species in this sample. This may signal the formation of oxidative intermediates such as sulfate radicals ($SO_4^{\bullet-}$), with Ag^+ cations acting as catalytic initiators potentially promoting the generation of these radicals alongside Ag_2^+ cations, as reported elsewhere.[29] While the exact mechanism is not fully elucidated, reduced sulfur-centered radicals confined within the zeolite framework (inset, Fig. 2A) could contribute to the transformation of the sulfate species under the applied synthesis conditions, comprising grinding PL-SOD, aqueous Ag^+ exchange in the dark, and mild drying at 50 °C. These intermediates may subsequently promote the formation of reactive oxygen species, which facilitate water oxidation and contribute to the reduction of Ag^+ to form Ag–NCs.[29]

This process may also contribute to a self-cleaning effect, whereby SO_4^{2-} ions are progressively consumed or transformed within the zeolite under the applied synthesis conditions. Similar behavior has been previously observed in the pulsed radiolysis generation of Ag–NCs in solution employing Ag_2SO_4 salts, where SO_4^{2-} anions acted as catalysts accelerating the clustering process of the NCs.[30] However, the Ag–NCs formed in solution exhibited limited stability due to the lack of structural confinement.

Ag K-edge XEOL–XAFS

In a second stage we used a combination of XEOL and transmission-detected Ag K-edge XAFS measured simultaneously to extensively characterize the structure and electronic properties of both dark and luminescent Ag species in Ag/S-zeolites. While conventional transmission-detection (Tr-EXAFS)[12,31–33] is a powerful method for investigating NC size and atomic-scale structures,[34] the information obtained refers to both dark and luminescent species. In contrast, the XEOL–EXAFS technique provides information specifically on the local structures of luminescent species.

Ag-K edge XANES spectra obtained using XEOL (Fig. 2B) and transmission (Fig. 2C) modes of as-synthesized Ag-exchanged S-zeolites (W_R@Ag/S, W_B@Ag/S, and W_W@Ag/S) display a related profile that clearly differs from that of SOD-Ag that features a more intense WL associated with a blue-shift of its edge position. Only minor differences between the XANES profiles obtained with the two detection methods are visible. In the Tr-XANES spectra, a limited redshift of the edge position of W_R@Ag/S, W_B@Ag/S, and W_W@Ag/S relative to that of the SOD-Ag reference sample (inset, Fig. 2C) is observed, whereas the edge position remains unaltered in the corresponding XEOL–XANES spectra (inset, Fig. 2B). This indicates that the non-luminescent single Ag co-cations are slightly more reduced in the white emitting Ag/S samples than in the SOD-Ag reference material probably due to a different zeolite environment that could result from the distinct method used to synthesize the latter sample.[12] The comparative analysis between the two detection modes presented in the SI (Fig. S2) shows that the XEOL mode systematically detects a slightly lower average Ag oxidation state than the transmission mode, indicating that the luminescent Ag atoms forming the cluster are slightly more reduced than the non-luminescent single Ag co-cations, in line with previous observations of different Ag species coordination environments.[11]

Phase-corrected Fourier Transforms (FTs) of W_B@Ag/S, W_W@Ag/S, and W_R@Ag/S, along with SOD-Ag (Fig. 3) of XEOL–XAFS (Fig. S3), display two main peaks. The first peaks are fitted with 1.0, 1.9, 2.2, and 2.5 oxygen atoms at distances of 2.15, 2.20, 2.30, and 2.38 Å in W_B@Ag/S, W_W@Ag/S, W_R@Ag/S, and SOD-Ag, respectively. This indicates that the luminescent Ag–NCs are coordinated to a variable number of ligands, consisting either of O atoms in W_B@Ag/S, W_W@Ag/S, and W_R@Ag/S, where the Ag_C–O distances are relatively short (2.15 to 2.30 Å), or of water molecules in SOD-Ag, which features a longer Ag_C–O distance (2.38 Å) in line with the Ag_C–(OH_2) distance of 2.36 Å detected in similar Ag–NCs confined in LTA-zeolites.[11] This excludes a direct coordination of the luminescent Ag–NCs to the sulfur atoms present in the Ag/S-zeolites. This is also supported by S K-edge S-XANES analysis that shows very similar profiles for W_W@Ag/S and its S precursor sodalite (PL-SOD) (Fig. 2A). The two profiles differ mainly in the intensity of the SO_4^{2-} peak at 2482.4 eV,[25,35] which is sharply reduced in the Ag-exchanged sample, suggesting that the sulfate originally present in the precursor material has been consumed, probably to oxidize the water molecules facilitating the formation of O–O bonds and the reduction of Ag^+ co-cations, as previously discussed.[29] This results in the formation of Ag–NCs coordinated to O atoms in the sodalite cages at a temperature as low as 50 °C, whereas in the absence of sulfur in the initial zeolite precursor (SOD-Ag), Ag–NCs are coordinated to water molecules.

The second multipeaks of the FTs were fitted with 2.5, 2.9, 3.7, and 3.8 Ag atoms at distances of 2.65, 2.74, 2.79, and 2.84 Å in W_B@Ag/S, W_W@Ag/S, W_R@Ag/S, and SOD-Ag, respectively, indicating that Ag atoms formed luminescent few-atom NCs within the sodalite cages in all samples. The non-integer number of Ag atom coordination numbers (CN_{AgC}s) indicates that Ag atoms assemble in all samples into mixtures of two or more NC sizes, ranging from Ag_3 (CN_{AgC} = 2) to Ag_6 (CN_{AgC} = 4), including Ag_4 (CN_{AgC} = 3) and possibly Ag_5 (CN_{AgC} = 3.3). The occurrence of different NC sizes is in line with the

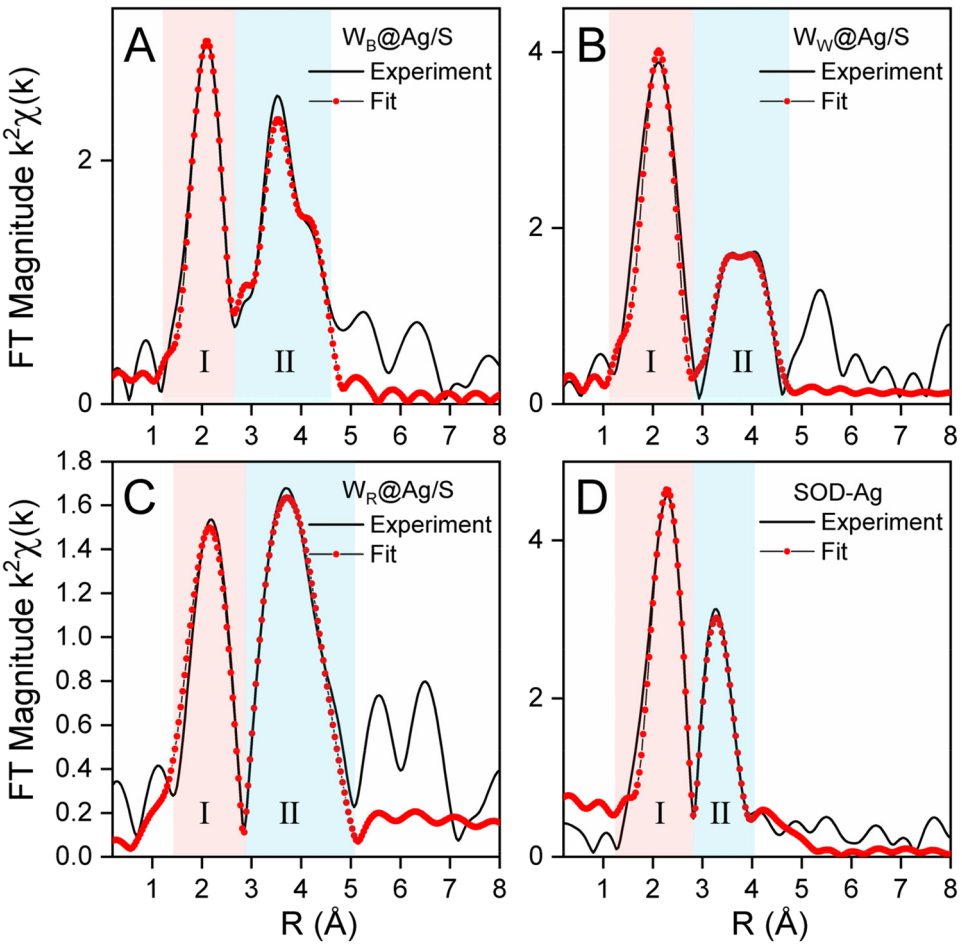

Fig. 3 XEOL-detected Ag K-edge k^2-weighted phase corrected FTs of (A) W_B@Ag/S, (B) W_W@Ag/S, (C) W_R@Ag/S, and (D) SOD-Ag best fits. The shaded peaks correspond to Ag_C–O (I-red) and Ag_C–Ag_C (II-blue) bond distances, indicating an oxygen coordination and the formation of luminescent Ag–NCs of varying sizes.

increase of the Ag_C–Ag_C bond distance with the Ag coordination number or NC size, from 2.65 to 2.84 Å. The presence of a mixture of different NC sizes is further supported by the very large Debye–Waller factors (DWFs) associated with the Ag_C–Ag_C shells (0.07–0.11 $Å^{-2}$) in all Ag/S-zeolites, which suggest a significant heterogeneity in the luminescent NC distances and a large level of static disorder. In contrast, the more standard DWF (0.03 $Å^{-2}$) observed in SOD-Ag suggests that a more homogeneous NC size distribution occurs in the SOD-Ag framework.

A half–half mixture of Ag_3 (CN_{AgC} = 2) and Ag_4 (CN_{AgC} = 3) yielding an average CN_{AgC} of 2.5 is the most natural solution for W_B@Ag/S, although the presence of a small fraction of larger NCs cannot be excluded. In W_W@Ag/S, the CN_{AgC} of 2.9 may indicate the presence of a single Ag_4 (CN_{AgC} = 3) NC; however, the very large DWF (0.11 $Å^{-2}$) and the white luminescence properties of this material strongly suggest the formation of a mixture of *ca.* 25% Ag_3 (CN_{AgC} = 2), 50% Ag_4 (CN_{AgC} = 3), and 25% Ag_6 (CN_{AgC} = 4), possibly also including Ag_5 (CN_{AgC} = 3.3). In W_R@Ag/S (CN_{AgC} = 3.7), a mixture of *ca.* 30% Ag_4 and 70% Ag_6 and/or a mixture of *ca.* 50% Ag_5 and 50% Ag_6 is likely composed of the luminescent NCs. Finally, the luminescent species in SOD-Ag consist of a large majority of Ag_6, including a few Ag_4/Ag_5 NCs, in line with the relatively small DWF determined in this material.

The coordination of the O ligands (CN_{OL}) surrounding the Ag–NCs corresponds neither to integer numbers of O atoms nor to water molecules inside the sodalite cage due to the co-existence of several oxygen atoms or water stoichiometries. The CN_{OL} of 1 in W_B@Ag/S suggests the presence of a single O-capping Ag_3O NC and a mixture of tetrahedral Ag_4O and Ag_4O_2 NCs, corresponding to a CN_{OL} of 0.75 and 1.5, respectively. In W_W@Ag/S, the average CN_{OL} of 1.9 would correspond to a mixture of Ag_3O, Ag_4O_2, and Ag_6O_4 NCs, while in W_R@Ag/S, the CN_{OL} of 2.2 matches with a mixture of Ag_4O_2 and Ag_6O_4 NCs. Finally, in SOD-Ag, the CN_{OL} of 2.5 may correspond to a mixture of $Ag_6(OH_2)_2$, $Ag_6(OH_2)_4$, and $Ag_6(OH_2)_6$ isomers.[11] These structures featuring an Ag_C–Ag_C interatomic distance of 2.84 Å are in line with those predicted by DFT calculations for hydrated Ag_6 NCs confined within sodalite-type cavities of fully Ag-exchanged LTA zeolites.[36] Luminescent Ag–NCs confined in the sodalite cage of the SOD material are likely all facially co-

ordinated with 1 to 4 oxygen atoms or water molecules. These NC geometries are in line with those reported in $Ag_4(H_2O)_x$ (x = 2 & 4) NCs confined in fully exchanged FAU-Ag and in partially exchanged LTA-Ag_3K_9 zeolites.[11]

Additionally, the XEOL–EXAFS fit was completed with two shells at longer distances consisting of 2.2 to 2.5 Ag at 3.35–3.4 Å (N_4) and 2 to 4.4 Ag at 3.60 to 3.96 Å (N_5). These shells correspond to distances between the Ag_C forming the NCs in the center of the sodalite and the surrounding Ag_R cations positioned in the single six-membered rings (S6Rs) of the same sodalite cage. N_4 corresponds to an Ag_C–Ag_R shell when an O_L atom is positioned between the NC and Ag_R, while the longer Ag_C–Ag_R distances in N_5 are found in the absence of O_L between the two atoms (Fig. S4). Unlike in LTA zeolites, where they can be positioned in the supercages linking the sodalite cages, the Ag_R cations in SOD zeolites are directly positioned between two neighboring NCs (Fig. 4 and Table S1 in the SI for details).[12] Due to the limited available space in SOD, most of the Ag_C–Ag_R distances are distributed around the average distances determined for the N_4 and N_5 shells, resulting in large DWFs from 0.01 to 0.06 $Å^{-2}$. The long Ag_C–Ag_R distances around 4.4 Å, typically found in LTA zeolites, only occur in limited cases in the SOD framework (Fig. S5).

Tr-EXAFS captures signals from both dark and luminescent species, showing a distinct profile from XEOL–EXAFS (Fig. S6), which provides more direct insights into the nuclearity and geometry of NCs within the sodalite cages. Ag–NCs with

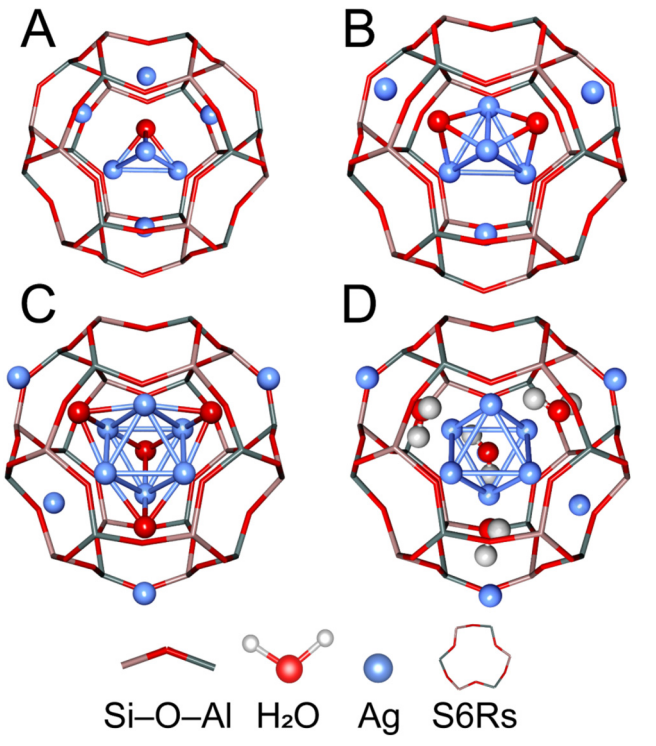

Fig. 4 Proposed structures of Ag_3O (A), Ag_4O_2 (B), Ag_6O_4 (C), and $Ag_6(OH_2)_4$ (D) NCs embedded in the sodalite cage, including the surrounding Ag_R cations located in the S6Rs. These structures are based on XEOL analysis and are intended solely as illustrative models.

average CN_{AgC} values of 2.5, 3.2, 3.5, and 4 in W_B@Ag/S, W_W@Ag/S, W_R@Ag/S, and SOD-Ag, respectively, derived from the Tr-EXAFS fitting parameters presented in Table S2, are in very good agreement with the CN_{AgC} values of 2.5, 2.9, 3.7, and 3.8 determined by XEOL–EXAFS. The corresponding intra-NC distances of 2.61, 2.71, 2.71, and 2.74 Å for W_B@Ag/S, W_W@Ag/S, W_R@Ag/S, and SOD-Ag, respectively, are systematically shorter and more uniform than those determined by XEOL. This is in line with previous DFT and XEOL–EXAFS investigations on similar Ag_4-NCs confined in the sodalite cages of LTA zeolites, which reported a significant increase of the intra-NC Ag_C–Ag_C distances from the ground state to the excited state, suggesting that XEOL–EXAFS selectively measures the excited-state structure.[11]

Tr-EXAFS provides additional information on the dark species present in the luminescent sodalites. While similar fractions of *ca.* 77 to 85% of Ag_C forming the Ag–NCs are positioned in the sodalite cages of SOD-Ag, single Ag_R cations located on the axis of the sodalite S6Rs account for the 15 to 23% remaining fractions of Ag atoms. Compared to LTA-Ag zeolites that present a typical Ag atom distribution of *ca.* 60% Ag_C (NC) and 40% Ag_R, the halved fractions of Ag_R observed in the SOD-Ag zeolites result from the SOD specific structure, where, unlike in LTA-Ag, the S6Rs are systematically shared between two neighboring sodalite cages. The CN_{OL} values of the Ag_C forming the Ag–NCs of 1.2, 1.8, 2.2, and 3.1 derived from the transmission data are in line with 1.0, 1.9, 2.2, and 2.5 determined by XEOL in W_B@Ag/S, W_W@Ag/S, W_R@Ag/S, and SOD-Ag, respectively.

The contribution of Ag_C–Ag_R shells (N_4 and N_5) to the fit indicates that, both in Ag/S-zeolites and SOD-Ag, all Ag–NCs confined in the sodalite cages are systematically surrounded by Ag_R cations. This confirms that most of the Na^+ co-cations that preferentially occupy this position were exchanged by Ag^+ in the synthesis process and highlights the remarkable Ag aggregation in the SOD structure, as already observed in Ag-zeolite structures.[37] The nearly equal distribution of Ag–NCs with different sizes may be dictated by the Ag_R cations located in the S6R axis, positioned outside the cage for Ag_6 and inside the cages for Ag_3 and Ag_4 NCs (Fig. 4), suggesting that an alternation of Ag_6 and Ag_4/Ag_3 NCs is the most efficient and stable NC organization in SOD zeolites, unlike in LTA zeolites, where the presence of supercages confers more flexibility in accommodating different NC sizes in contiguous cages.[12]

The formation of O_L-coordinated Ag–NCs, likely due to the presence of SO_4^{2-} anions within the zeolite structure, facilitates the stabilization of an Ag–NC network. These Ag–NCs do not rehydrate under ambient conditions likely due to the closed structure of SOD, characterized by the absence of a supercage network (Fig. S5) preventing the diffusion of water into the zeolite structure observed in LTA and FAU zeolites. Moreover, the O_L that also coordinates the Ag_R cations in the rings to one or two Ag–NCs may form stronger, bi-directional bonds than water molecules that are strongly polarized, further contributing to the NC stabilization.[38] In this context, the initial S doping of the SOD precursor not only influences the Ag–NC structure but also plays a key role in their stabiliz-

ation. This effect may stem from a redistribution of electronic density between the Ag–NCs and the zeolite framework, along with changes in the local electrostatic potential that influence coulombic interactions, similar to those induced by small cations such as Li^+, which modulate the electronic orbitals of NCs in the excited state.[13] Therefore, fine-tuning the chemical environment enables control over both the NC distribution and the material's optical response.

This structural investigation demonstrates that the multi-tone white luminescence of Ag-exchanged S-SOD originates from the formation and stabilization of precise fractions of Ag–NCs of different nuclearities, ranging from Ag_3 to Ag_6, coexisting inside the zeolite structure. Previous studies on Ag-exchanged LTA zeolites have indeed shown that the emission wavelength of few-atom Ag–NCs formed in sodalite cages upon activation systematically increased with respect to the NC nuclearity. The blue emission observed in LTA partially exchanged with lithium (Li-LTA) and with low Ag loadings has been associated with low-nuclearity Ag–NCs (Ag_3), identified through EXAFS spectroscopy.[37] In fully Li-exchanged LTA, EXAFS analysis revealed the formation of a stable $Ag_4(O)_2$–$[Li^+]_6^{m+}$ species after dehydration, responsible for the green emission of these samples.[39] Finally, the red/orange luminescence of heat-treated, highly Ag-loaded LTA zeolites was attributed to Ag_6^{m+} NCs in LTA zeolites.[7]

Considering the structural and optical similarities of these systems, it is reasonable to associate the species present in our samples with those described in LTA zeolites. We previously showed that the electronic structure of hydrated $Ag_4(H_2O)_x$ clusters formed in the sodalite cages of Ag-K-LTA zeolites consists of a confined two-electron superatom quantum system with hybridized Ag and water O orbitals delocalized over the cluster. Their frontier orbitals are composed of a contribution of up to 25% from the O states of the surrounding framework O and H_2O ligands.[11] As Ag_4O_2 clusters possess similar structures and optical properties to their hydrated counterparts, we hypothesize that a similar electronic structure prevails when the water ligands are replaced by O atoms in the sodalite cages of SOD zeolites.

The cold bluish-white luminescence of W_B@Ag/S can be attributed to an equimolar mixture of blue-emitting Ag_3O and a combination of green-emitting tetrahedral Ag_4O and Ag_4O_2 NCs coexisting in this material. The more neutral white emission of W_W@Ag/S can be attributed to the more balanced distribution of *ca.* 25% of blue-emitting Ag_3O, 50% green-emitting Ag_4O_2 NCs, and 25% red-emitting Ag_6O_4. Meanwhile, the warm reddish-white emission of the W_R@Ag/S sample is due to the combination of *ca.* 30% of green-emitting Ag_4O_2 and a large fraction of 70% red-emitting Ag_6O_2.

In contrast, SOD-Ag exclusively emits in the narrow yellowish-orange region (Fig. 1B), as only red-emitting Ag_6 NCs coordinated with water molecules—corresponding to a mixture of $Ag_6(OH_2)_2$, $Ag_6(OH_2)_4$, and $Ag_6(OH_2)_6$ isomers—are formed in this structure. Furthermore, the absence of sulfur in the precursor SOD leads to the formation of a more uniform distribution of emissive species preventing the spectral blending necessary for white emissions. Unlike more open structures such as LTA or FAU, where multiple-emitter configurations are less stable due to a lower level of confinement and the tendency to form large, disordered NCs at high Ag contents, the closed topology of SOD, combined with the chemistry induced by S doping, provides an exceptionally effective framework for stabilizing a network of Ag–NCs. This makes Ag/S-SOD zeolites promising platforms for the rational design of multi-tone white emitters in confined systems.

Unlike FAU or LTA zeolites, where Ag–NCs coordinated to highly mobile water molecules tend to form Ag nanoparticles after activation or undergo rapid degradation of the highly luminescent species under X-ray beam exposure,[39,40] the Ag/S-SOD samples preserved their structural and optical integrity. The remarkable structural and optical stability of the white Ag/S-SOD samples enabled their analysis through advanced techniques such as XEOL–XAFS and XANES, even under harsh conditions such as high energy doses and long exposure times.[40] This allows the establishment of a direct correlation between the emissive species and their atomic environments, highlighting the effectiveness of the synthesis and activation procedures employed. This also demonstrates a clear relationship between the atomic-scale structure and the broadband white emission, advancing the fundamental understanding of luminescent Ag–NCs in zeolitic hosts. The structural and optical robustness of these white-emitting Ag/S-SOD materials further makes them attractive candidates for practical applications. In fact, they have been previously demonstrated as single-phase phosphors in remote LED prototypes,[20] where thin phosphor layers (10–20 μm) efficiently convert NUV excitation into white light, with EQE values around 19% and CIE coordinates close to pure-white-light emission (0.33, 0.33). The detailed structural insights provided in the present study can guide the rational design and optimization of such phosphor materials for solid-state lighting and other optoelectronic devices.

Conclusions

Using the innovative XEOL–EXAFS, we successfully identified and characterized the structure of luminescent Ag–NCs in white-emissive Ag/S-zeolite samples. The analysis revealed a heterogeneous mixture of Ag–NCs coordinated with oxygen ligands (Ag_3O, Ag_4O_2, and Ag_6O_4), varying in size and coordination. Ag–O and Ag–Ag bond distances indicate distinct coordination environments and NC assemblies, depending on the material (W_B@Ag/S, W_W@Ag/S, and W_R@Ag/S). This suggests that the interaction between Ag^+ and SO_4^{2-} anions may facilitate the formation of reactive intermediates, potentially contributing to the water oxidation and to the stabilization of Ag–NCs of various nuclearities coordinated to oxygen ligands within the zeolite cavities, unlike in S-free zeolites, where Ag–NCs coordinated to water ligands are formed. The coexistence of multiple Ag–NC species with varied O_L coordination, forming a stable network within the closed structure of the SOD zeolite, leads to a broad distribution of emissive species that collectively display white luminescence. The precise color temperature can

be further tuned by controlling the respective fractions of the different emitting species. These findings offer detailed insights into the structure and the chemical factors governing white-light emission in zeolite-based phosphors and open pathways for designing advanced luminescent materials with tailored functionalities across diverse applications.

Author contributions

J. A. Moreno-Torres, C. Viola, and A. Ruivo prepared the samples and conducted the experiments with the help of P. Thompson and C. A. T. Laia. Francesco D'Acapito, P. Lievens, D. Grandjean, and E. Coutiño-Gonzalez conceived and designed the experiments. D. Grandjean, J. A. Moreno-Torres, and E. Coutiño-Gonzalez prepared the manuscript with the help of all co-authors, who have given their approval to the final version of the manuscript.

Conflicts of interest

The authors declare no competing financial interest.

Data availability

The data related to this article are shown in the figures and the supplementary information (SI). The raw data related to these figures will be available on KU Leuven institutional research data repository (https://rdr.kuleuven.be/dataverse/rdr) at https://doi.org/10.48804/7QZBE.

Supplementary information: zeolite characterization. See DOI: https://doi.org/10.1039/d6nr00693k.

Acknowledgements

E. C.-G. gratefully acknowledges the financial support from FWO through the research stay grant V502522N. This research was also funded by the FCT-Portuguese Foundation for Science and Technology, through the grants UID/00729/2025 (https://doi.org/10.54499/UID/00729/2025); LA/P/0140/2020, Puc-LED – PTDC/CTM-CTM/0757/2021, UID/50006/2025, and 2020.00252.CEECIND. The authors thank the ESRF for providing beamtimes (CH-4818 and CH-5465) and the staff of LISA-BM08 and XMAS-BM28 for their assistance during the measurements.

References

1 A. Oliden-Sánchez, R. Sola-Llano, J. Pérez-Pariente, L. Gómez-Hortigüela and V. Martínez-Martínez, *Int. J. Mol. Sci.*, 2024, **25**, 3577.
2 A. Gonzàlez-Rosell, C. Cerretani, P. Mastracco, T. Vosch and S. M. Copp, *Nanoscale Adv.*, 2021, **3**, 1230–1260.
3 J. Ren, S. Zhou, P. Hu, P. Meng and Z. Zhang, *Dalton Trans.*, 2025, **54**, 4213–4224.
4 H. S. Lim, S. G. Jeong, G. B. Park, J. Y. Kim, N. H. Heo and W. T. Lim, *Inorg. Chem.*, 2024, **63**, 13991–14003.
5 S. Zong, B. Wang, J. Zhang, X. Yu, Y. Zhou, Y. Chen, T. Zhang and J. Li, *Angew. Chem., Int. Ed.*, 2025, **64**, e202420156.
6 Y. Zhang, L. Han, B. Li, H. Li and Y. Xu, *Laser Photonics Rev.*, 2025, **00529**, 1–10.
7 G. De Cremer, E. Coutiño-Gonzalez, M. B. J. Roeffaers, B. Moens, J. Ollevier, M. Van Der Auweraer, R. Schoonheydt, P. A. Jacobs, F. C. De Schryver, J. Hofkens, D. E. De Vos, B. F. Sels and T. Vosch, *J. Am. Chem. Soc.*, 2009, **131**, 3049–3056.
8 M. Gutiérrez, Y. Zhang and J. C. Tan, *Chem. Rev.*, 2022, **122**, 10438–10483.
9 E. Coutiño-Gonzalez, W. Baekelant, J. A. Steele, C. W. Kim, M. B. J. Roeffaers and J. Hofkens, *Acc. Chem. Res.*, 2017, **50**, 2353–2361.
10 G. Romolini, J. A. Steele, J. Hofkens, M. B. J. Roeffaers and E. Coutino-Gonzalez, *Adv. Opt. Mater.*, 2021, **9**, 1–13.
11 D. Grandjean, E. Coutiño-Gonzalez, N. T. Cuong, E. Fron, W. Baekelant, S. Aghakhani, P. Schlexer, F. D'Acapito, D. Banerjee, M. B. J. Roeffaers, M. T. Nguyen, J. Hofkens and P. Lievens, *Science*, 2018, **361**, 686–690.
12 O. Fenwick, E. Coutiño-Gonzalez, D. Grandjean, W. Baekelant, F. Richard, S. Bonacchi, D. De Vos, P. Lievens, M. Roeffaers, J. Hofkens and P. Samorì, *Nat. Mater.*, 2016, **15**, 1017–1022.
13 W. Baekelant, S. Aghakhani, E. Coutino-Gonzalez, K. Kennes, F. D'Acapito, D. Grandjean, M. Van Der Auweraer, P. Lievens, M. B. J. Roeffaers, J. Hofkens and J. A. Steele, *J. Phys. Chem. Lett.*, 2018, **9**, 5344–5350.
14 D. Yao, S. Xu, Y. Wang and H. Li, *Mater. Chem. Front.*, 2019, **3**, 1080–1084.
15 J. A. Moreno-Torres, A. Lecharlier, F. Espejel-Ayala, J. Hofkens, E. Fron, M. B. J. Roeffaers, E. Coutino-Gonzalez and R. Ramírez-Bon, *ACS Appl. Nano Mater.*, 2024, **7**, 11965–11972.
16 H. Li, D. Yao, Y. Wang and P. Li, *Dalton Trans.*, 2020, **49**, 8179–8185.
17 D. Yao, J. Yang, Y. Xie, Y. Wang, Y. Wang and H. Li, *J. Alloys Compd.*, 2020, **823**, 153778.
18 H. Gao, D. Chen, G. Fang, S. Yuan, X. Chen and J. Zhong, *J. Alloys Compd.*, 2018, **764**, 17–23.
19 C. Viola, C. A. T. Laia, M. Outis, L. F. V. Ferreira, L. C. Alves, M. Teixeira, F. Folgosa, J. C. Lima, A. Ruivo and J. Avó, *Mater. Today Chem.*, 2023, **30**, 101514.
20 W. Baekelant, G. Romolini, L. Sun, M. De Ras, E. Fron, T. Moreira, C. Viola, A. Ruivo, C. A. T. Laia, J. Martens, C. Martin, C. W. Kim, M. Van Der Auweraer, M. B. J. Roeffaers, J. Hofkens and E. Coutino-Gonzalez, *Methods Appl. Fluoresc.*, 2020, **8**, 024004.
21 A. Ruivo, E. Coutino-Gonzalez, M. M. Santos, W. Baekelant, E. Fron, M. B. J. Roeffaers, F. Pina, J. Hofkens and C. A. T. Laia, *J. Phys. Chem. C*, 2018, **122**, 14761–14770.

22 F. D'Acapito, A. Trapananti, S. Torrengo and S. Mobilio, *Notiziario Neutroni e Luce di Sincrotrone*, 2014, **19**, 1592–7822.
23 N. Binsted, J. Campbell, S. J. Gurman and P. C. Stephenson, *EXAFS analysis Programs,* SERC Daresbury Laboratory EXCURVE Program, Warrington, U.K., 1991.
24 P. B. J. Thompson, B. N. Nguyen, R. Nicholls, R. A. Bourne, J. B. Brazier, K. R. J. Lovelock, S. D. Brown, D. Wermeille, O. Bikondoa, C. A. Lucas, T. P. A. Hase and M. A. Newton, *J. Synchrotron Radiat.*, 2015, **22**, 1426–1439.
25 J. Goettlicher, A. Kotelnikov, N. Suk, A. Kovalski, T. Vitova and R. Steininger, *Z. Kristallogr. – Cryst. Mater.*, 2013, **228**, 157–171.
26 J. M. Carvalho, I. Norrbo, R. A. Ando, H. F. Brito, M. C. A. Fantini and M. Lastusaari, *Chem. Commun.*, 2018, **54**, 7326–7329.
27 M. Ganio, E. S. Pouyet, S. M. Webb, C. M. Schmidt Patterson and M. S. Walton, *Pure Appl. Chem.*, 2018, **90**, 463–475.
28 A. A. Gambardella, M. Cotte, W. de Nolf, K. Schnetz, R. Erdmann, R. van Elsas, V. Gonzalez, A. Wallert, P. D. Iedema, M. Eveno and K. Keune, *Sci. Adv.*, 2020, **6**, eaay8782.
29 L. Yu, J. Wang, D. Guo, W. You, M. Liu, L. Zhang and C. Li, *Dalton Trans.*, 2015, **44**, 710–717.
30 P. Mulvaney and A. Henglein, *Chem. Phys. Lett.*, 1990, **168**, 391–394.
31 T. Miyanaga, Y. Suzuki, N. Matsumoto, S. Narita, T. Ainai and H. Hoshino, *Microporous Mesoporous Mater.*, 2013, **168**, 213–220.
32 T. Yamamoto, S. Takenaka, T. Tanaka and T. Baba, *J. Phys.: Conf. Ser.*, 2009, **190**, 012171.
33 A. Kulesza, R. Mitrić, V. Bonačić-Koutecký, B. Bellina, I. Compagnon, M. Broyer, R. Antoine and P. Dugourd, *Angew. Chem., Int. Ed.*, 2011, **50**, 878–881.
34 M. L. Neidig, J. Sharma, H. C. Yeh, J. S. Martinez, S. D. Conradson and A. P. Shreve, *J. Am. Chem. Soc.*, 2011, **133**, 11837–11839.
35 A. A. Gambardella, C. M. Schmidt Patterson, S. M. Webb and M. S. Walton, *Microchem. J.*, 2016, **125**, 299–307.
36 N. T. Cuong, H. M. T. Nguyen, M. P. Pham-Ho and M. T. Nguyen, *Phys. Chem. Chem. Phys.*, 2016, **18**, 18128–18136.
37 E. Coutino-Gonzalez, W. Baekelant, D. Grandjean, M. B. J. Roeffaers, E. Fron, M. S. Aghakhani, N. Bovet, M. Van Der Auweraer, P. Lievens, T. Vosch, B. Sels and J. Hofkens, *J. Mater. Chem. C*, 2015, **3**, 11857–11867.
38 S. Aghakhani, D. Grandjean, W. Baekelant, E. Coutiño-Gonzalez, E. Fron, K. Kvashnina, M. B. J. Roeffaers, J. Hofkens, B. F. Sels and P. Lievens, *Nanoscale*, 2018, **10**, 11467–11476.
39 W. Baekelant, S. Aghakhani, E. Fron, C. Martin, C. Woong-Kim, J. A. Steele, T. De Baerdemaeker, F. D'Acapito, D. Chernysov, M. Van Der Auweraer, P. Lievens, D. Grandjean, M. Roeffaers, J. Hofkens and E. Coutino-Gonzalez, *J. Mater. Chem. C*, 2019, **7**, 14366–14374.
40 E. Coutino-Gonzalez, D. Grandjean, M. Roeffaers, K. Kvashnina, E. Fron, B. Dieu, G. De Cremer, P. Lievens, B. Sels and J. Hofkens, *Chem. Commun.*, 2014, **50**, 1350–1352.